Research Article

FEM Analyses for T-H-M-M Coupling Processes in Dual-Porosity Rock Mass under Stress Corrosion and Pressure Solution

Yu-Jun Zhang,[1] Chao-Shuai Yang,[2] and Gang Xu[1]

[1] *State Key Laboratory of Geomechanics and Geotechnical Engineering, Institute of Rock and Soil Mechanics, The Chinese Academy of Sciences, Wuhan 430071, China*
[2] *Technology Centre, China Railway Tunnel Group Co. Ltd., Luoyang 471009, China*

Correspondence should be addressed to Chao-Shuai Yang, yangchaoshuai2008@126.com

The models of stress corrosion and pressure solution established by Yasuhara et al. were introduced into the 2D FEM code of thermo-hydro-mechanical-migratory coupling analysis for dual-porosity medium developed by the authors. Aiming at a hypothetical model for geological disposal of nuclear waste in an unsaturated rock mass from which there is a nuclide leak, two computation conditions were designed. Then the corresponding two-dimensional numerical simulation for the coupled thermo-hydro-mechanical-migratory processes were carried out, and the states of temperatures, rates and magnitudes of aperture closure, pore and fracture pressures, flow velocities, nuclide concentrations and stresses in the rock mass were investigated. The results show: the aperture closure rates caused by stress corrosion are almost six orders higher than those caused by pressure solution, and the two kinds of closure rates climb up and then decline, furthermore tend towards stability; when the effects of stress corrosion and pressure solution are considered, the negative fracture pressures in near field rise very highly; the fracture aperture and porosity are decreases in the case 1, so the relative permeability coefficients reduce, therefore the nuclide concentrations in pore and fracture in this case are higher than those in case 2.

1. Introduction

The rock mass below thousands of meters from the ground surface, which is dual-porosity medium with pore and fracture as the conduits of transporting, will be the site for the recovery of energy resources and minerals, and for the safe isolation and storage of high level radioactive wastes, CO_2, and so forth. So, the changes in the ambient stress and temperature conditions may affect the permeability characteristics of these conduits combined effects. Stress corrosion [1–4] and pressure solution [5–8], which are corresponding to the fractures,

may result in the sealing and degradation of permeability through compaction driven by fracturing (or crushing) of the propping asperities and by dissolution at contacting asperities, respectively.

When local tensile stresses result from the compressive loading of contacting asperities, "subcritical" or "quasistatic" cracking may occur, leading to a time-dependent or progressive failure. Specifically, sub-critical crack growth in the presence of water is believed to be facilitated by chemical reaction, and the resulting process is termed stress corrosion. Pressure solution incorporates three serial processes: mineral dissolution at stressed contacts, diffusive transport of this material along the intervening thin film of water, and ultimate deposition of the mineral matter at the pore wall.

Dove [9] rigorously investigated the dissolution kinetics of quartz under the wide range of temperature and pH conditions and defined an empirical expression of mode I crack velocity resulted from chemical dissolution. Based on the experimental data, Yasuhara and Elsworth [10] investigated the evolution of fracture aperture within a sample of novaculite containing a natural fracture, and they also presented the models which separately account for stress corrosion and pressure solution to describe this response. Taron and Elsworth [11] introduced a kind of coupled thermo-hydro-mechanical-chemical model of dual-porosity medium, in which the influence of pressure solution, shrinkage and dilation of T-H-M, and precipitation and dissolution of mineral on the opening and closure of apertures was considered by simplification. Subsequently, on the basis of modifying permeability and porosity, the characteristics and change mechanisms of permeability within a rock mass containing natural fractures with TOUGHREACT and FLAC^{3D} were investigated. Taron and Elsworth [12, 13] developed a new model of pressure solution and applied it for numerical simulation of coupled mechanical and chemical processes in engineered geothermal reservoirs with dynamic permeability. Using simplified expression developed by Min et al. [14], the author improved the FEM code of T-H-M coupling of dual-porosity medium, modified the aperture timely and established the evolution of fracture permeability with pressure solution. Aiming at a hypothetical nuclear waste repository in an unsaturated dual-porosity rock mass as the calculation example, the relative numerical simulation [15] was carried out for three cases with different apertures. However, the concentration field of solute was not involved. It is well known that the leakage and diffusion of nuclide from nuclear waste repository are required to study [16]. Consequently, it is imperative to improve the existing model and FEM code, and to perform the analyses of T-H-M-M coupling based on the above work.

The author introduced primarily the models of stress corrosion and pressure solution by Yasuhara into the governing equations presented in [15], and the concentration of solute was involved as well. That is, in the dual-porosity rock mass, the stress field and the temperature field were single, but the water pressures both in pore and fracture are different as well as the concentrations. Therefore, the corresponding simulation for T-H-M-M coupling was constructed. And then, aiming at a hypothetical model for geological disposal of nuclear waste in an unsaturated dual-porosity rock mass, two computation cases were designed: (1) the fracture apertures were changed with the stress corrosion and pressure solution (the porosity of intact rock was also a function of stress); (2) the fracture aperture and the porosity of matrix rock were constants. The corresponding FEM analyses were performed under certain initial conditions of temperature, pore water pressure, in situ stress, and nuclide release intensity, and both the distributions and the changes of temperatures, pore pressures, flow rates, saturations, nuclide concentrations, and stresses in the near field of repository were investigated. Some conclusions were obtained.
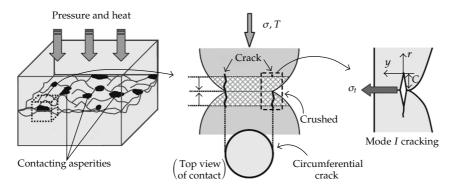
Figure 1: Schematic of fracture compaction induced by microcrack propagation [10].

2. Modification of Fracture Permeability

2.1. Effect of Stress Corrosion on Aperture

Assume that the asperity contacts of brittle materials, schematically shown in Figure 1, within a fracture are in Hertzian contacts, and that a circumferential crack at or outside the contact may be induced by the tensile stress σ_t. And this crack is described as stress corrosion. Mode I crack velocity for quartz was defined by Dove, given as [9]

$$
\begin{aligned}
v_{\text{Si-O}} = {} & A_{\text{H}_2\text{O}} \exp\left(\frac{-\Delta H_{\text{H}_2\text{O}}}{RT}\right) \exp\left(b^*_{\text{H}_2\text{O}} K_1\right)\left(\theta^{\text{H}_2\text{O}}_{\text{Si-O}}\right) \\
& + A_{\text{OH}^-} \exp\left(\frac{-\Delta H_{\text{OH}^-}}{RT}\right) \exp\left(b^*_{\text{OH}^-} K_1\right)\left(\theta^{\text{OH}^-}_{\text{Si-O}}\right),
\end{aligned}
\tag{2.1}
$$

where $v_{\text{Si-O}}$ is mode I crack velocity caused by chemical dissolution; $A_{\text{H}_2\text{O}}$ and A_{OH^-} are the experimentally-determined factor related to temperature; $\Delta H_{\text{H}_2\text{O}}$ and ΔH_{OH^-} are activation enthalpies; R is the gas constant; T is temperature; $b^*_{\text{H}_2\text{O}}$ and $b^*_{\text{OH}^-}$ are the experimentally determined constants derived from the geometry of crack tip; K_1 is the stress intensity factor; $\theta^{\text{H}_2\text{O}}_{\text{Si-O}}$ and $\theta^{\text{OH}^-}_{\text{Si-O}}$ always satisfying $\theta^{\text{H}_2\text{O}}_{\text{Si-O}} + \theta^{\text{OH}^-}_{\text{Si-O}} = 1$ are the fraction of Si–O reacting with molecular water or hydroxyl ions, and there will be $\theta^{\text{H}_2\text{O}}_{\text{Si-O}} = 1$ and $\theta^{\text{OH}^-}_{\text{Si-O}} = 0$ at low pH, and $\theta^{\text{H}_2\text{O}}_{\text{Si-O}} = 0$ and $\theta^{\text{OH}^-}_{\text{Si-O}} = 0$ at the high one. Consequently, the closure rate of fracture mechanical aperture due to stress corrosion, given by Yasuhara and Elsworth [10], is as follows:

$$
\begin{aligned}
\frac{dE^s}{dt} &= -(1 - R_c) \cdot v_{\text{Si-O}}, \\
K_1 &\approx \sigma_t \sqrt{2\pi r}, \\
\sigma_t &= -\frac{(1 - 2\mu)}{2}\sigma_a, \\
\sigma_a &= \frac{\overline{R}}{R_c}\overline{\sigma},
\end{aligned}
\tag{2.2}
$$

where r is the distance parallel to the long axis direction of mode I crack caused by σ_t, and it is assumed to be infinitesimal as well as initial length of crack; μ is the Poisson's ratio of material; σ_t is the tensile stress induced by σ_a which reaches the maximum value just at the edge of the contact; σ_a is the real stress exerted over the contact area; $\overline{\sigma}$ is average macroscopic effective stress. $\overline{R}$ is the nominal area of the fracture (taking unit value); R_c is the contact-area ratio, and $R_c \leq \overline{R}$.

R_c can be calculated via the expression below:

$$E^s = E_r + (E_0 - E_r) \exp[-(R_c - R_{c0})a], \tag{2.3}$$

where E^s and E_r are the mean and residual apertures caused by stress corrosion, respectively; E_0 is the initial aperture; R_{c0} is the relative contact-area ratio at the reference stress; a is empirical constant.

Therefore, the evolution of fracture mechanical aperture derived from stress corrosion is

$$E_{t+\Delta t}^s = E_t^s + \frac{dE^s}{dt}\Delta t. \tag{2.4}$$

2.2. Effect of Pressure Dissolution on Aperture

The dissolution defined by Yasuhara and Elsworth [10] is expressed as

$$\frac{dM_{\text{diss}}}{dt} = \frac{3\pi V_m^2(\sigma_a - \sigma_c)k_+\rho_g d_c^2}{4RT}, \tag{2.5}$$

where dM_{diss}/dt is the rate of addition of dissolved mass into solution at the interface; V_m is molar volume of the solid; σ_c is the critical stress that defines stress state where the compaction will effectively halt and reach equilibrium while σ_a is equal to σ_c; k_+ is the dissolution rate constant of the solid; ρ_g is the density of solid; d_c is the diameter of the asperity contact.

And

$$k_+ = k_+^0 \exp\left(-\frac{E_a}{RT}\right),$$
$$\sigma_c = \frac{E_m(1 - T/T_m)}{4V_m}, \tag{2.6}$$

where k_+^0 is constant factor; E_a is the activation energy; E_m and T_m are the heat and temperature of fusion, respectively.

The closure rate of fracture mechanical aperture caused by pressure solution is

$$\frac{dE^p}{dt} = -\frac{dM_{\text{diss}}}{dt} \cdot \frac{1}{\rho_g} \cdot \frac{1 - R_c}{(\pi/4)d_c^2} = -\frac{3V_m^2 k_+^0(1 - R_c)(\sigma_a - \sigma_c)}{RT} \exp\left(-\frac{E_a}{RT}\right). \tag{2.7}$$

And the evolution of fracture mechanical aperture due to pressure solution can be expressed as

$$E^p_{t+\Delta t} = E^p_t + \frac{dE^p}{dt}\Delta t. \tag{2.8}$$

2.3. Fracture Permeability

The fracture spacing in rock mass is assumed to be s, and then the total mechanical aperture for a single fracture at the time of $t + \Delta t$ is expressed as

$$E_{t+\Delta t} = \left(E_0 + \sum_{\Delta t} dE^s + \sum_{\Delta t} dE^p \right). \tag{2.9}$$

So, the hydraulic aperture for a single fracture is [17]

$$e_{t+\Delta t} = \frac{E^2_{t+\Delta t}}{\mathrm{JRC}^{2.5}}, \tag{2.10}$$

where JRC is the roughness coefficient of fractures.

Consequently, the equivalent permeability coefficient of fracture in rock mass is [18]:

$$K_{t+\Delta t} = \frac{ge^3_{t+\Delta t}}{12vs}, \tag{2.11}$$

where g is gravitational acceleration ($9.81\,\mathrm{m/s^2}$) and v is kinematics viscosity (the magnitude relative to purified water at 20°C is $1.0 \times 10^{-6}\,\mathrm{m^2/s}$).

2.4. Effect of Stress on Permeability of Rock Matrix

According to the empirical expression presented by J. P. Davies and D. K. Davies [19], the porosity and permeability of the rock matrix, when the stress in rock matrix changes, can be modified as

$$\phi = \phi_r + (\phi_0 - \phi_r)\exp(f \cdot \sigma'_m),$$
$$k = k_0 \exp\left[c \cdot \left(\frac{\phi}{\phi_0} - 1 \right) \right] = F_{\phi k}k_0, \tag{2.12}$$

where ϕ_0 and k_0 are the porosity and permeability of rock matrix at the stress state of zero, respectively; ϕ_r is the residual porosity of rock matrix at a high stress state; σ'_m is average effective stress; f and c are the experimentally determined parameters, respectively; $F_{\phi k}$ is the modification factor of pore permeability.
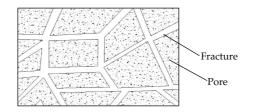
Figure 2: Porous-fractured media.

3. Thermo-Hydro-Mechanical-Migratory Coupling Equations for Dual-Porosity Medium

For the dual-porosity medium shown in Figure 2, it can be thought that there exist pore water pressure and fracture water pressure, pore concentration and fracture concentration, but stress field and temperature field are single in the medium. So, one kind of three-dimensional model for coupled thermo-hydro-mechanical-migratory process is created. By omitting the complex deriving steps, the governing equations are given as follows.

3.1. Equilibrium Stress Equation

Supposing there are n sets of fractures in a fractured porous rock mass, the equilibrium stress equation can be written in the global coordinate system as below:

$$
\frac{d\sigma}{dt} = D\left[\frac{d\varepsilon}{dt} - m\left(C_1 - \frac{1}{3K_s}\right)(s_{w1} + D_{s1}p_{w1})\frac{dp_{w1}}{dt}\right.
$$
$$
\left. - m\left(C_2 - \frac{1}{3K_s}\right)(s_{w2} + D_{s2}p_{w2})\frac{dp_{w2}}{dt} - m\frac{\beta_S}{3}\frac{dT}{dt}\right],
$$
(3.1)

where σ and ε are the total stress and total stain, respectively; $D = (C_1 + C_2)^{-1}$ is the elastic matrix; $m^T = [1\ \ 1\ \ 0]$ is the unit normal column matrix; K_s, β_S, and T are the bulk modulus, synthesized thermal expansion coefficient, and temperature of the fractured porous rock mass, respectively; s_{w1}, p_{w1}, D_{s1}, C_1 and s_{w2}, p_{w2}, D_{s2}, C_2 are the saturation degree, water pressure, specific moisture content, and flexibility matrix of rock matrix and fractured network, respectively; t is the time.

3.2. Continuity Equation for Groundwater

On the basis of the principle of mass balance, the water volume flowing into an object during a time increment of dt is equal to the rate of water accumulation within the object. Assuming that the seepage of water can be expressed by Darcy law, the continuity equation for rock matrix is expressed by

$$
- \nabla^T\left\{k_1\frac{k_{rw1}}{\mu_w}\nabla(p_{w1} + \gamma_w z)\right\} + \frac{\overline{\alpha}k_1 k_{rw1}}{\mu_w}(p_{w1} - p_{w2})
$$
$$
+ A_1\frac{\partial\varepsilon}{\partial t} + B_1\frac{\partial p_{w1}}{\partial t} + E_1\frac{\partial p_{w2}}{\partial t} + F_1\frac{\partial T}{\partial t} - \nabla^T D_{t1}\nabla T = 0,
$$
(3.2)

where k_1 and k_{rw1} are the intrinsic permeability tensor and relative permeability of rock matrix, respectively; ρ_w, μ_w, and γ_w are the density, dynamic viscosity and unit weight of water, respectively; z is the head above some arbitrary datum; $\overline{\alpha}$ is a parameter determined by the aperture and geometry of fracture; D_{t1} is the thermal water diffusivity of rock matrix; and A_1, B_1, E_1, and F_1 are the constant matrixes.

For the fractured medium, the continuity equation of groundwater is:

$$
\begin{aligned}
-\nabla^T \left\{ k_2 \frac{k_{rw2}}{\mu_w} \nabla\left(p_{w2} + \gamma_w z\right) \right\} - \frac{\overline{\alpha} k_1 k_{rw1}}{\mu_w}\left(p_{w1} - p_{w2}\right) \\
+ A_2 \frac{\partial \varepsilon}{\partial t} + B_2 \frac{\partial p_{w2}}{\partial t} + E_2 \frac{\partial p_{w1}}{\partial t} + F_2 \frac{\partial T}{\partial t} - \nabla^T D_{t2} \nabla T = 0,
\end{aligned}
\tag{3.3}
$$

where k_2 and k_{rw2} are the intrinsic permeability tensor and relative permeability of fractured medium, respectively; A_2, B_2, E_2 and F_2 can be obtained by replacing subscripts 1 and 2 in expressions of A_1, B_1, E_1 and F_1 with subscripts 2 and 1; D_{t2} is the thermal water diffusivity of fractured medium.

3.3. Energy Conservation Equation

In accordance with the principle of energy conservation, the rate of heat flowing into an object equals the increase of the internal energy within the object. The temperature field is single, and the energy conservation equation takes the form below:

$$
\begin{aligned}
-\nabla^T \lambda \nabla T + \left(s_{w1}\phi_1 V_1^a + s_{w2}\phi_2 V_2^a\right)\rho_w C_w \left(\nabla^T T\right) \\
+ \left[(1-\varphi_1)C_s T \frac{\rho_s}{K_s} \varphi_1 C_w T \frac{\rho_w}{K_w} \right]\left(s_{w1} + D_{s1}p_{w1}\right)\frac{\partial p_{w1}}{\partial t} \\
- \left\{ (1-\varphi_1)C_s T \rho_s \beta_s + (\varphi_1 + \varphi_2)C_w T \rho_w \beta_w - \left[(1-\varphi_1)\rho_s C_s + (\varphi_1+\varphi_2)\rho_w C_w\right] \right\}\frac{\partial T}{\partial t} \\
+ \frac{1}{2}(1-\phi_1)\beta_s T \frac{\partial}{\partial t}\left(u_{i,j} + u_{j,i}\right)\delta_{ij} = 0,
\end{aligned}
\tag{3.4}
$$

where C_w is the specific heat of water; C_s, ρ_s, and λ are the specific heat, density and thermal conductivity matrix of fractured porous rock mass, respectively; V_1^a and V_2^a are the apparent flow velocities of pore water and fracture water, respectively; u_i and u_j are the displacement components; δ_{ij} is the Kronecker's delta.

3.4. Percolation-Migration Equation

The percolation-migration equation in [20] was improved by us with the new meaning of adding the solute exchange between rock matrix and fractured network due to concentration

difference. The new percolation-migration equation is derived from the old one as follows:

$$R_i\theta_i\rho_w\frac{\partial c_i}{\partial t} = \nabla^T\theta_i\rho_w D_i\nabla c_i - \theta_i\rho_w V_i\nabla c_i - R_i\theta_i\rho_w\chi c_i + (-1)^{i+1}\overline{\omega}\theta_i\rho_w D_1(C_1 - C_2) - Q_{c_i}, \quad (3.5)$$

where $i = 1, 2$ correspond to rock matrix and fractured network, respectively; R_i is the retardation coefficient and is defined as $R_i = V_i/V_i^* = (1 + (\rho_{di}/\theta_i)K_{di})$; V_i is the apparent velocity of groundwater; V_i^* is the transport velocity of radioactive nuclide; ρ_{di} is the dry density of rock matrix or fractured network; K_{di} is the distribution coefficient for saturated media; V_i is the apparent velocity of groundwater; θ_i the volumetric water content; D_i is the diffusion tensor; c_i is the concentration of solute; V_i is the apparent velocity vector of groundwater; χ is the radioactive decay constant; $\overline{\omega}$ is the coefficient which depends on the fracture aperture and geometry; Q_{c_i} is the source term.

The diffusion tensor can be given by

$$D_{i\alpha\beta} = \alpha_{iT}|V_i|\delta_{\alpha\beta} + (\alpha_{iL} - \alpha_{iT})\frac{V_{i\alpha}V_{i\beta}}{|V_i|} + \alpha_{im}\tau_i\delta_{\alpha\beta}, \quad (3.6)$$

where α_{iT} is the transversal dispersivity; α_{iL} is the longitudinal dispersivity; $|V_i|$ is the absolute value of the apparent flow velocity; α_{im} is the molecular diffusion coefficient; τ_i is the tortuosity coefficient; $\delta_{\alpha\beta}$ is the Kronecker's delta.

The discretizations both in space and time domains are carried out for the equilibrium equation, the continuity equation, the energy conservation equation, and the percolation-migration equation by Galerkin method, and then the FEM pattern can be obtained.

The models of stress corrosion and pressure dissolution developed by Yasuhare et al. were introduced into the governing equations above for T-H-M coupling in dual-porosity rock mass by the author, and the corresponding algorithm was consulted in [21, 22].

4. Computation Example

The computation model in laboratory scale is shown in Figure 3. A canister filled with the vitrified radioactive nuclear waste is disposed at a certain depth beneath the ground surface, and the surrounding rock mass is quartzite which is also an unsaturated dual-porosity medium. As an approximate simplification, it is treated to be a plane strain problem. A computation region with a horizontal length of 4 m and a vertical length of 8 m is taken. There are 800 elements and 861 nodes in the mesh. From the midpoint at the right margin of the vitrified waste to right, the node numbers are 432, 433, 434, 435, and 436, respectively. The boundary conditions are as follows.

The free displacement is allowed for the top of computation domain over which the vertical distributed load of σ_v = 26.7 MPa is exerted; both the left and right sides are fixed horizontally; the bottom face is fixed vertically; on all the boundary faces the pore pressure, fracture pressure, and temperature are constant with values of −4.59 MPa, −0.46 MPa, and 20°C, respectively. There exist one set of horizontal fractures and one group of vertical ones in the rock matrix, separately. The state of coupled T-H-M is to act as the role of stress corrosion and pressure solution on the fracture aperture. The relative calculating parameters are tabulated in Tables 1, 2 (The parameter values in these two tables are assumed by the authors, but they have reasonable orders.), and Table 3 (All the parameters in this table are taken from
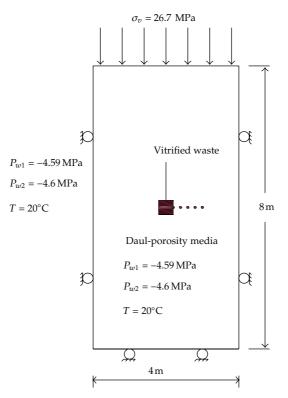
Figure 3: Computation model.

[10] except R_{c0}, $\overline{R}$, and JRC.). The saturations of rock matrix and fracture system are 0.44 and 0.01, respectively, and the temperature of rock mass is the uniform value of 20°C at the initial state. The waste continuously releases heat with a constant power of 1000 W during a period of 4 years [23].

The water retention curves of both porous and fracture media conform to the Van Genuchten model, that is,

$$s_w = (s_{ws} - s_{wr})(1 + |\alpha\psi|^n)^{-m} + s_{wr}, \qquad (4.1)$$

where $\alpha = 3.86 \times 10^{-6}\,\mathrm{m}^{-1}$, $n = 1.41$ for the rock matrix; $\alpha = 5.26 \times 10^{-4}\,\mathrm{m}^{-1}$, $n = 2.55$ for the fracture system; $m = 1 - 1/n$; ψ is the water potential head; s_{ws} is the maximum saturation with a value of 1.0 while s_{wr} is the minimum saturation of which the values are 0.19 for the rock mass and 0.01 for the fracture system, respectively.

The relationship between relative permeability and saturation degree is

$$k_{rw} = s_w^{2.0}. \qquad (4.2)$$

Both the thermal water diffusivities of the rock matrix and fracture system are taken as

$$D_t = 2.5 \times 10^{-10}\,\mathrm{m}^2/\mathrm{s}°\mathrm{C}. \qquad (4.3)$$

Table 1: Main computation parameters.

Property	Rock mass	Vitrified waste
Density, ρ (kN·m^{-3})	26.7	25.0
Porosity, ϕ_1	0.11	0.0
Permeability, k_1/μ_w (m^2·Pa^{-1}·s^{-1})	1.24×10^{-13}	1.0×10^{-27}
Young's modulus, E (GPa)	37.0	53.0
Poisson's ratio, μ	0.3	0.25
Specific heat, C (kJ·kg^{-1} · °C^{-1})	1.0	0.7
Thermal expan. coeff., β (°C^{-1})	8.8×10^{-6}	1.0×10^{-5}
Thermal conductivity, λ (W·m^{-1} · °C^{-1})	2.8	5.3

Table 2: Parameters for fracture sets used in calculation.

Parameter	Horizontal fracture	Vertical fracture
Spacing, S (m)	0.3	0.3
Continuity ratio, l	1	1
Dip angle, θ(°)	0	90
Normal stiffness, k_n (MPa/m)	1000.0	2000.0
Shearing stiffness, k_s (MPa/m)	500.0	1000.0
Porosity, ϕ_2	0.01	0.01
Permeability, k_2/μ_w (m^2/Pa·s)	9.7×10^{-9}	9.7×10^{-9}

Table 3: Parameters for stress corrosion and pressure solution.

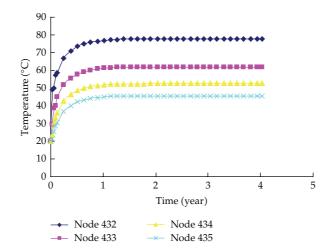| Parameter	Unit	Values
Empirical constant, a	—	5.0
Origin asperity contact-area ratio, R_{c0}	—	0.1
Nominal asperity contact-area ratio, $\overline{R}$	—	1.0
Roughness coefficient of fracture, JRC	—	2.5
Factor, A_{H_2O}	ms^{-1}	1.12×10^{-4} T
Factor, A_{OH^-}	ms^{-1}	2.51×10^3 T
Origin aperture, E_0	m	0.0125
Residual aperture, E_r	m	0.0025
Constant, $b^*_{H_2O}$	N^{-1} m$^{3/2}$	2.69×10^{-5} (quartz)
Constant, $b^*_{OH^-}$	N^{-1} m$^{3/2}$	1.78×10^{-5} (quartz)
Activation energy, E_a	J·mol^{-1}	7.0×10^4 (quartz)
Heat of fusion, E_m	J·mol^{-1}	8.57×10^3 (quartz)
Activation enthalpy for H$_2$O, ΔH_{H_2O}	J·mol^{-1}	6.6×10^4
Activation enthalpy for OH$^-$, ΔH_{OH^-}	J·mol^{-1}	8.27×10^4
Reference dissolution rate constant, k_+^0	mol·m^{-2} s^{-1}	1.59
Infinitesimal distance from crack tip, r	m	1.0×10^{-6}
Gas constant, R	J·mol^{-1} K^{-1}	8.31
Temperature of fusion, T_m	K	1883 (quartz)
Molar volume, V_m	m^3 mol^{-1}	2.27×10^{-5} (quartz)
Fraction of Si–O reacting with H$_2$O, $\theta_{Si-O}^{H_2O}$	—	0.99921 (pH = 7)
Fraction of Si–O reacting with OH$^-$, $\theta_{Si-O}^{OH^-}$	—	0.00079 (pH = 7)

Figure 4: Temperatures versus time at some nodes for case 1.

The vitrified waste is the source term with a diffusive mass flux of radioactive nuclides $Q_{c1} = 1.44 \times 10^{-10}$ mol·kg/m³·s⁻¹. The constants used in the computation concerned with the percolation-migration of nuclide are supposed as follows: the tortuosity coefficients τ_1, τ_2 are 0.4 and 0.8, respectively; the dispersivities in the longitudinal direction α_{1L} and α_{2L} are 1.0 m and 2.0 m, respectively; the dispersivities in the transversal direction are $\alpha_{iT} = \alpha_{iL}/10$; the molecular diffusion coefficients α_{1m} and α_{2m} are 1.0×10^{-9} m²/s and 2.0×10^{-9} m²/s, respectively; the distribution coefficients K_{d1} and K_{d2} are 8.0 mL/g and 5.3 mL/g, respectively; the dry densities ρ_{d1} and ρ_{d2} are 23.0 kg/m³ and 21.0 kg/m³, respectively; the parameter $\overline{\omega}$ is 100.0 m⁻²; the radioactive decay constant $\chi = \ln 2/T_{\text{half}}$, where T_{half} is the half life of radioactive nuclide and is taken as 1000 years in the computation. The waste radiates continuously heat with a power of 1000 W during a period of 4 years, and the time step is taken as 100000 s.

For the two cases with different evolutions of fracture aperture above, the change and distribution of the temperatures, displacements, pore pressures, nuclide concentrations and stresses in the rock mass are studied. The analyses of the main computation results are as follows.

The changes of temperatures in calculation region for case 1 and 2 are basically the same. Taking case 1 for instance, the temperatures versus time at nodes 432, 433, 434, and 435 are shown in Figure 4. In the early 0.1 a, the temperature of buffer increases fast, then it grows slowly. At the termination of computation, the temperatures of nodes 432, 433, 434, and 435 are 77.8°C, 62.0°C, 52.5°C, and 45.7°C, respectively.

Induced by the stress corrosion and pressure dissolution, the aperture closure rates of the horizontal fracture and the vertical fracture at the midpoint on the right edge of the canister versus time are plotted in Figures 5 and 6, respectively. It can be seen that both the rates due to these two factors climb up, then decline after the peak, and furthermore tend towards stability slowly. The aperture closure rates caused by stress corrosion are almost six orders higher than those caused by pressure solution. This response is similar with the conclusions presented in [10]. Meanwhile, the aperture closure rates of horizontal fractures are larger than those of vertical fractures, and the reason is that the vertical stresses are higher than the horizontal ones in rock mass. The apertures and the asperity contact-area ratios of
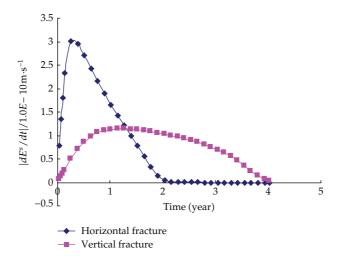
Figure 5: $|dE^s/dt|$ caused by stress corrosion versus time at middle point of right margin of vitrified waste.
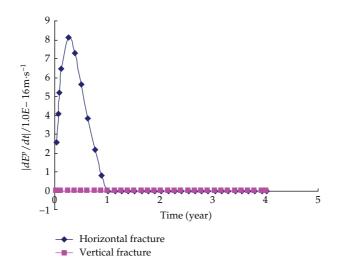

Figure 6: $|dE^p/dt|$ caused by pressure solution versus time at middle point of right margin of vitrified waste.

the horizontal fracture and the vertical fracture at the midpoint mentioned above versus time are presented in Figures 7 and 8, respectively. For the former, the apertures decrease from the original value and then tend towards the residual value. The contact-area ratios of asperities increase also from initial value then towards the nominal value (unit value), and the changes of the values corresponding to the horizontal fractures are more significant. It can be seen in Figure 9 that stress intensity factor ratio on vertical crack is much larger than that on horizontal crack at this midpoint, and both of them reduce over time. It is shown in Figure 10 that at this midpoint, the critical stresses of horizontal fracture and vertical fracture are equal. They decline rapidly at the beginning, and then tend towards constant. This phenomenon is just due to the combined effects of temperature, stress, and chemistry.
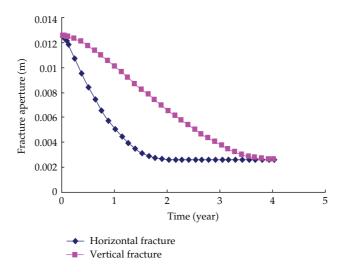
Figure 7: Fracture apertures versus time at middle point of right margin of vitrified waste.
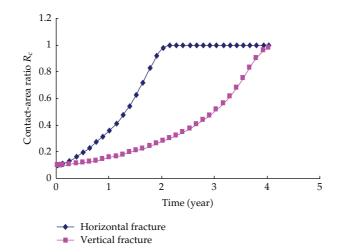

Figure 8: Contact-area ratios versus time at middle point of right margin of vitrified waste.

Pore and fracture pressures at nodes 432, 433, 434, and 435 versus time for case 1 and case 2 are presented in Figures 11 and 12, respectively. It can be seen that negative pore and fracture pressures rise higher for case 1 than those for case 2. Particularly, at node 432 where the effects of stress corrosion and pressure solution are the most intense, the negative fracture pressure reaches a quite large value. The reason of this response is that the reduction of stress corrosion and pressure dissolution on the fracture apertures and the change of pore permeability with time are considered for case 1, while the fracture apertures and the pore permeability remain constants for case 2. The negative pore and fracture pressures at node 432 at 4 a are −12.25 MPa, −7.95 MPa for case 1 and −6.03 MPa, −0.66 MPa for case 2, respectively. Contours of pore and fracture pressures within a range of 2 m × 2 m around the canister at 4 years for case 1 and case 2 are described in Figures 13 and 14, respectively. It is found that the
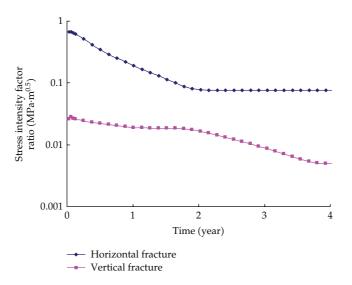
Figure 9: Stress intensity factor ratios versus time at middle point of right margin of vitrified waste.
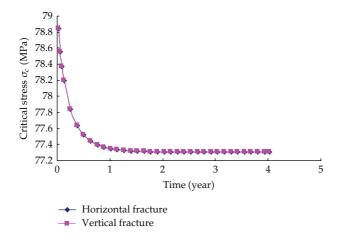

Figure 10: Critical stresses versus time at middle point of right margin of vitrified waste.

fracture pressures affected by the stress corrosion and pressure dissolution for case 1 have a significant growth around the canister as compared with case 2.

The flow vector distributions of pore and fracture water in calculation domain at 4 a for the two cases are presented in Figure 15. The fracture flow vectors for case 1, on which the effects of stress corrosion and pressure dissolution are considered, are quite distinguished from those for case 2, especially in the vicinity of canister. Taking the node 432 for instance, flow velocities of pore and fracture are 3.40×10^{-8} m/s, 1.52×10^{-8} m/s for case 1 and 2.32×10^{-8} m/s, 2.77×10^{-8} m/s for case 2, respectively.

Pore and fracture concentrations at nodes 432, 433, 434, and 435 versus time for the two cases are presented in Figures 16 and 17, respectively. Compared with case 2 in which all of the aperture, porosity, and pore permeability are constants, the nuclides both in fracture and pore are gathered largely in case 1 for the reason that both the reduction of aperture
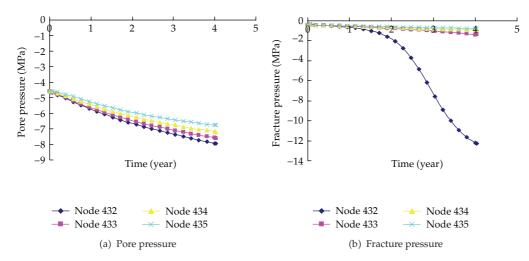
(a) Pore pressure

(b) Fracture pressure

Figure 11: Pore and fracture water pressures versus time at some nodes for case 1.

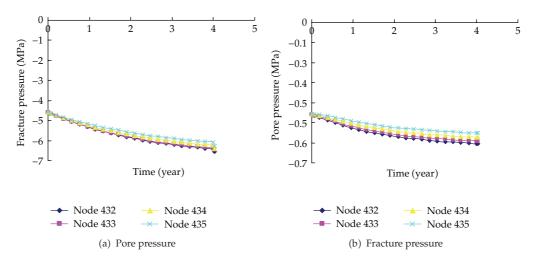(a) Pore pressure

(b) Fracture pressure

Figure 12: Pore and fracture water pressures versus time at some nodes for case 2.

due to stress corrosion and pressure dissolution and the compression of porosity due to mean effective stress lead to decreasing the permeabilities of pore and fracture. The nuclide concentrations at nodes 432, 433, 434, and 435 at 4 a for the two cases are 20.18/6.82, 15.42/3.60, 12.06/2.55 and 9.36/1.76 for rock matrix, and 10.86/8.44, 8.39/6.82, 6.28/5.54 and 5.00/4.63 for fracture system, respectively, (the values in the left and right of "/" are for case 1 and 2, resp., and their units are 10^{-3} mol/m^3). Contours of pore and fracture concentrations within a range of 2 m × 2 m around the canister at 4 years for case 1 and case 2 are described in Figures 18 and 19, respectively.

The differences between the magnitudes and distributions of stresses within the rock mass in the two cases are quite small for the reason that the impacts of negative pore pressure and negative fracture pressure on the mechanical balance are not considered [24]. For instance, normal stress contours in calculation domain at 4 a for case 1 are given in Figure 20.
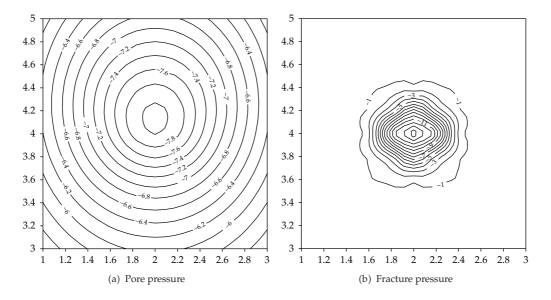
(a) Pore pressure   (b) Fracture pressure

Figure 13: Contours of pore and fracture pressures in a 2 m × 2 m area at 4 years for case 1 (MPa).

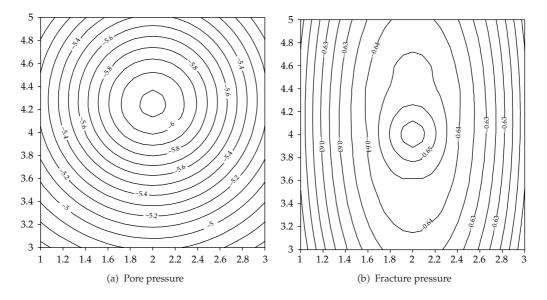(a) Pore pressure   (b) Fracture pressure

Figure 14: Contours of pore and fracture pressures in a 2 m × 2 m area at 4 years for case 2 (MPa).

It can be known that the stress fields, influenced by the existence of the vitrified waste and the effect of radiating heat, are distinguished from those caused only by the gravity of rock mass (the contours of the latter are the horizons). At 4 a, the horizontal stress and vertical stress at the midpoint on the right edge of the canister are −0.124 MPa and −26.75 MPa, respectively. The compressive effect is not to be analyzed in this paper.
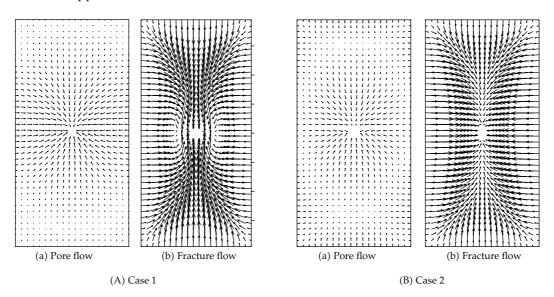
(a) Pore flow (b) Fracture flow

(A) Case 1

(a) Pore flow (b) Fracture flow

(B) Case 2

Figure 15: Flow vectors of pore and fracture water in calculation domain at 4 years.

(a) Pore concentration
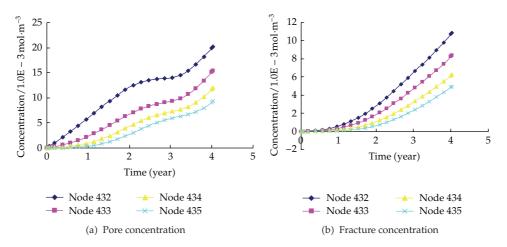
(b) Fracture concentration

Figure 16: Nuclide concentrations versus time at some nodes for case 1.

5. Concluding Remarks

Based on the introduction of stress corrosion and pressure dissolution of fracture aperture as well as the concentration field of solute, the existing governing equations for T-H-M coupling in dual-porosity rock mass were developed to a model for T-H-M-M coupling. Taking a hypothetical model for geological disposal of nuclear waste with a nuclide leakage in an unsaturated dual-porosity rock mass as a calculation example, on the basis of the two cases whether the changes of fracture apertures with stress corrosion and pressure dissolution are considered or not (meanwhile whether the porosity of rock matrix is the stress function or not), the change and distribution of temperatures, rates and magnitudes of aperture closure, pore pressures, flow velocities, nuclide concentrations, and stresses in rock mass were
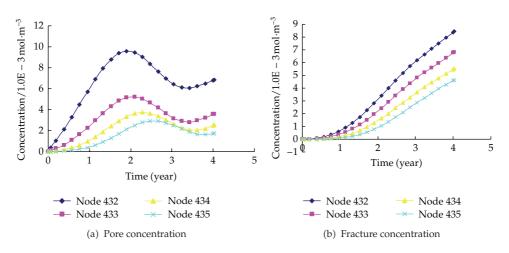
(a) Pore concentration

(b) Fracture concentration

Figure 17: Nuclide concentrations versus time at some nodes for case 2.

(a) Pore concentration
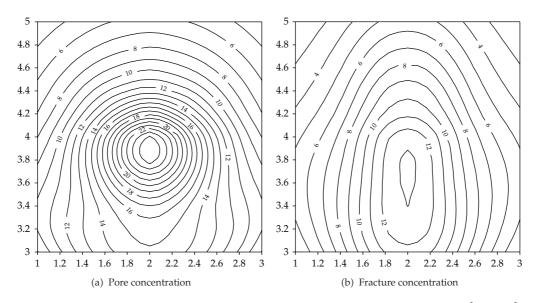

(b) Fracture concentration

Figure 18: Contours of nuclide concentration in a $2\,\text{m} \times 2\,\text{m}$ area at 4 years for case 1 (10^{-3} mol/m^3).

investigated by the two-dimensional FEM simulation for the coupled T-H-M-M processes. It is shown from the computing results that the temperature differences between case 1 and case 2 are not large, and the temperature in near field can reach 30.0~80.0°C at the end of calculation (4 a); the aperture closure rates caused by stress corrosion are almost six orders higher than those produced by pressure solution, and the two kinds of closure rates rise and then reduce, and furthermore tend towards stability; the fracture apertures decrease from the original value and tend towards the residual value while the contact-area ratios of asperities increase from the original value and tend towards the nominal value; the tensile stress and critical stress exerted over cracks decline over time and then tend towards constants; the negative fracture pressures for the case in which the effects of stress corrosion and pressure solution are considered in near field rise more highly than those for the case in which the
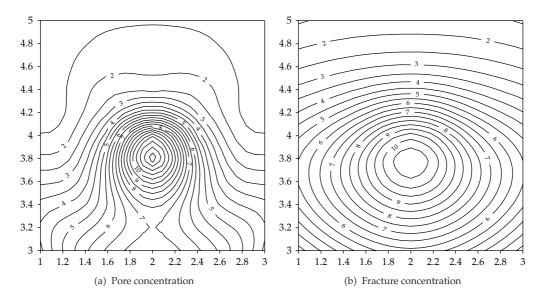
(a) Pore concentration   (b) Fracture concentration

Figure 19: Contours of nuclide concentration in a $2\,m \times 2\,m$ area at 4 years for case 2 ($10^{-3}\,mol/m^3$).

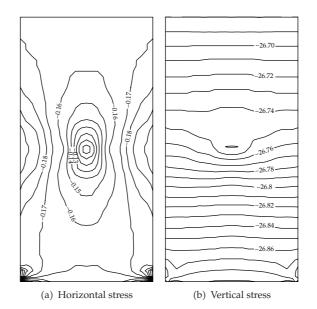(a) Horizontal stress   (b) Vertical stress

Figure 20: Normal stress contours in calculation domain at 4 years for case 1 (MPa).

corresponding effects are not considered, and the differences of flow vectors between the two cases are quite large; the permeabilities of fracture and pore decline resulted from stress corrosion, pressure dissolution, and mean effective stress in case 1, while they are constants in case 2, so the concentrations both in fracture and pore for the former are larger than those for the latter. but the differences between the magnitudes and distributions of stresses within the rock mass in two cases are very small.

However, the models of stress corrosion and pressure solution by Yasuhara et al. are based on the laboratory test for small scale rock, and the application of them in large-scale rock mass engineering remain to be examined. They are applied on FEM analysis with THMM coupling for a hypothetical model of geological disposal of nuclear waste in an unsaturated rock mass by the authors, and the reliability of it is limited in a certain extent. The further research remains to be carried out in the future.

Acknowledgments

References

[1] B. K. Atkinson, "A fracture mechanics study of subcritical tensile cracking of quartz in wet environments," *Pure and Applied Geophysics*, vol. 117, no. 5, pp. 1011–1024, 1979.

[2] P. M. Dove, "The dissolution kinetics of quartz in sodium chloride solutions at 25° to 300°C," *American Journal of Science*, vol. 294, no. 6, pp. 665–712, 1994.

[3] J. S. Chester, S. C. Lenz, F. M. Chester, and R. A. Lang, "Mechanisms of compaction of quartz sand at diagenetic conditions," *Earth and Planetary Science Letters*, vol. 220, no. 3-4, pp. 435–451, 2004.

[4] Y. Nara and K. Kaneko, "Study of subcritical crack growth in andesite using the Double Torsion test," *International Journal of Rock Mechanics and Mining Sciences*, vol. 42, no. 4, pp. 521–530, 2005.

[5] P. Y. F. Robin, "Pressure solution at grain-to-grain contacts," *Geochimica et Cosmochimica Acta*, vol. 42, no. 9, pp. 1383–1389, 1978.

[6] T. Dewers and A. Hajash, "Rate laws for water-assisted compaction and stress-induced water- rock interaction in sandstones," *Journal of Geophysical Research*, vol. 100, no. 7, pp. 13–112, 1995.

[7] A. Revil, "Pervasive pressure-solution transfer: a poro-visco-plastic model," *Geophysical Research Letters*, vol. 26, no. 2, pp. 255–258, 1999.

[8] H. Yasuhara, D. Elsworth, and A. Polak, "Evolution of permeability in a natural fracture: significant role of pressure solution," *Journal of Geophysical Research B*, vol. 109, no. 3, pp. B03204–11, 2004.

[9] P. M. Dove, "Geochemical controls on the kinetics of quartz fracture at subcritical tensile stresses," *Journal of Geophysical Research*, vol. 100, no. 11, pp. 22–359, 1995.

[10] H. Yasuhara and D. Elsworth, "Compaction of a rock fracture moderated by competing roles of stress corrosion and pressure solution," *Pure and Applied Geophysics*, vol. 165, no. 7, pp. 1289–1306, 2008.

[11] J. Taron and D. Elsworth, "Thermal-hydrologic-mechanical-chemical processes in the evolution of engineered geothermal reservoirs," *International Journal of Rock Mechanics and Mining Sciences*, vol. 46, no. 5, pp. 855–864, 2009.

[12] J. Taron and D. Elsworth, "Coupled mechanical and chemical processes in engineered geothermal reservoirs with dynamic permeability," *International Journal of Rock Mechanics and Mining Sciences*, vol. 47, no. 8, pp. 1339–1348, 2010.

[13] J. Taron and D. Elsworth, "Constraints on compaction rate and equilibrium in the pressure solution creep of quartz aggregates and fractures: controls of aqueous concentration," *Journal of Geophysical Research B*, vol. 115, no. 7, Article ID B07211, 2010.

[14] K. B. Min, J. Rutqvist, and D. Elsworth, "Chemically and mechanically mediated influences on the transport and mechanical characteristics of rock fractures," *International Journal of Rock Mechanics and Mining Sciences*, vol. 46, no. 1, pp. 80–89, 2009.

[15] Y. J. Zhang and W. Q. Zhang, "Finite element analysis of influence of pressure solution of fracture aperture on T-H-M coupling in dual-porosity medium," *Yantu Lixue/Rock and Soil Mechanics*, vol. 31, no. 4, pp. 1269–1275, 2010 (Chinese).

[16] E. Sonnenthal, A. Ito, N. Spycher et al., "Approaches to modeling coupled thermal, hydrological, and chemical processes in the drift scale heater test at Yucca Mountain," *International Journal of Rock Mechanics and Mining Sciences*, vol. 42, no. 5-6, pp. 698–719, 2005.

[17] R. Olsson and N. Barton, "An improved model for hydromechanical coupling during shearing of rock joints," *International Journal of Rock Mechanics and Mining Sciences*, vol. 38, no. 3, pp. 317–329, 2001.

[18] D. T. Snow, "Anisotropic permeability of fractured media," *Water Resources Research*, vol. 5, no. 6, pp. 1273–1289, 1969.

[19] J. P. Davies and D. K. Davies, "Stress-dependent permeability: characterization and modeling," in *Proceedings of the SPE Annual Technical Conference and Exhibition*, SPE 56813, Houston, Tex, USA, 1999.

[20] M. Nishigaki, "Density dependent transport analysis saturateds-unsaturated porous media—3 dimensional eulerian lagrangian method," Okayama University, 2001.

[21] Y. Zhang and W. Zhang, "3D thermo-hydro-mechanical-migratory coupling model and FEM analyses for dual-porosity medium," *Science China Technological Sciences*, vol. 53, no. 8, pp. 2172–2182, 2010.

[22] Y.-J. Zhang and C.-S. Yang, "coupled hermo-hydro-mechanical—migratory model for dual-porosity medium and numerical analysis," *Journal of Central South University of Technology*, vol. 18, no. 4, pp. 1256–1262, 2011.

[23] J. Rutqvist, B. Freifeld, K. B. Min, D. Elsworth, and Y. Tsang, "Analysis of thermally induced changes in fractured rock permeability during 8 years of heating and cooling at the Yucca Mountain Drift Scale Test," *International Journal of Rock Mechanics and Mining Sciences*, vol. 45, no. 8, pp. 1373–1389, 2008.

[24] M. Chijimatsu, H. Kurikami, A. Ito, and Y. Sugita, "Implication of THM coupling on the near-field of a nuclear waste repository in a homogeneous rock mass," DECOVALES III-Task3-Bench Mark Test 1(BMT1)-Subtask BMT1-B, pp.1–43, 2002.